PROGRESS IN COLOR, COLORANTS AND COATINGS

available online @ www.pccc.icrc.ac.ir

Prog. Color Colorants Coat. 10 (2017), 1-12

Ministry of Science, Research and Technology
Institute for Color Science and Technology

A Study of Oxidation Behavior of AZ91D Alloy with YSZ Coating Using EIS

A. Shahriari[1], H. Aghajani[*1], M. G. Hosseini[2]

[1.] Department of Materials Engineering, Faculty of Mechanical Engineering, University of Tabriz, P. O. Box: 51666-16471, Tabriz, Iran

[2.] Department of Physical Chemistry, Faculty of Chemistry, University of Tabriz, P. O. Box: 51666-16471, Tabriz, Iran

ARTICLE INFO

Article history:
Received: 2 Sep 2016
Final Revised: 30 Oct 2016
Accepted: 13 Nov 2016
Available online: 20 Dec 2016

Keywords:
Electrochemical impedance Spectroscopy
Oxide film
AZ91D
YSZ

ABSTRACT

Oxidation behavior of AZ91D magnesium alloy with 3YSZ coating and aluminum interlayer was studied in air at 250 °C using electrochemical impedance spectroscopy (EIS), scanning electron microscopy (SEM), and X-ray diffraction (XRD). The oxidation process was carried out in various times from 1 to 10 h. A three-electrode electrochemical cell was employed for all the EIS measurements. Also, to focus on the characteristics of the oxide films, a nonaggressive electrolyte (0.1 M Na_2SO_4) was used. The EIS data were interpreted with a two-layered model, and the obtained capacitance and resistance are related to the thickness and defectiveness of YSZ coating and oxide film which was formed during the oxidation process. The results showed that after 6 h of oxidation time, the defects are produced in YSZ coating and it helps to increase the thickness of the oxide film. Also, XRD results revealed that the oxide films were mainly composed of Al_2O_3 and $MgAl_2O_4$ phases. The oxide film remained protective during extra oxidation period. In addition, the electrochemical model was supported by SEM observations. Prog. Color Colorants Coat. 10 (2017), 1-12© Institute for Color Science and Technology.

1. Introduction

In the 21st century, resources of metals are limited, but magnesium is an abundant element that has some important characteristics such as low density and high strength-to-weight ratio. It could be used in many fields such as aerospace, automotive, and defense industries [1]. In addition, magnesium and its alloys are applied to household or electronic appliances [2]. However, poor corrosion resistance of magnesium and its alloys is a major disadvantage. This problem limits the development of these alloys as a commercial structure in industries. Many studies have focused on the corrosion mechanism of magnesium and its alloys [3].

Oxidation and aqueous corrosion of magnesium alloys are both electrochemical reactions. So, metal is changed to metal ion accompanied with electrons. Oxide and hydroxide layers spontaneously form on the surface of the magnesium and its alloys [1].

*Corresponding author: h_aghajani@tabrizu.ac.ir

Meanwhile, in terms of thermodynamic, magnesium is a very active element and the changes of standard Gibbs free energy (ΔG_0) of the magnesium oxidation are quite negative [4]. When magnesium and its alloys are exposed to an environment including oxygen or water, their surfaces have a great tendency to be oxidized. On the other hand, oxide or hydroxide could easily be formed on the surface of these alloys [5]. When the magnesium substrate contains traces of alloying elements, their oxides or hydroxides will become the constituents of the surface film [4]. For example, magnesium and aluminum hydroxides are the two main components of the surface film formed on AZ91D magnesium alloy [4]. Although, the microstructural model of aluminum and magnesium oxides are similar and both of them have a compact inner layer and a non-compact (porous) outer layer; the magnesium oxide is not protective as aluminum oxide [5]. Alloying of magnesium by some elements such as aluminum can increase the corrosion resistance of this metal by formation of a passive layer like Al_2O_3 with MgO and $Mg(OH)_2$ [4]. Furthermore, the corrosion protection of magnesium alloys can be improved by applying an inorganic coating that is pore-free and well-adhered to the substrate [6].

So far, various coating processes have been applied on magnesium and its alloys which have their own advantages and disadvantages. Application of inorganic coatings onto magnesium alloy surface can enhance its corrosion resistance in dry and aqueous corrosive medium. Among them, Yttria stabilized zirconia (YSZ) has low thermal conductivity and excellent surface properties [7]. It has generally been used for gas turbines and diesel engines in order to increase the operating temperature. In a previous study, YSZ coating was applied on magnesium alloy as an attempt to improve its corrosion resistance [8]. On the other hand, electrophoretic deposition (EPD) is one of the most outstanding techniques in order to deposit an inorganic coating on the metallic substrate. This technique has many advantages including high versatility that can be used with different materials, simplicity and cheap equipment [9]. Also, some interlayers such as aluminum can be applied in order to increase the quality and adherence of the inorganic coating to the magnesium substrate [10]. In addition, when a metallic bond layer is used between the substrate and top coating, it can be easily oxidized and defects can be formed on its surface. These defects together with stress concentration finally lead to failure of coatings [11].

When a protective coating is present, corrosion of the underlying metal is basically hindered. In this case, an important parameter for measurement of the corrosion resistance is electrical resistance of the oxides that are formed during the oxidation process [12, 13]. The presence of large defects such as pores, cracks, and channels inside the oxide films act as short-circuit paths for the oxidation reaction. These flaws have a strong influence on the electrical resistance of the oxide film and finally oxidation behavior of the metallic substrate [14].

Electrochemical impedance spectroscopy (EIS) can be used to investigate the electrical properties of different types of surfaces produce on the metallic substrates [15-18]. Recently, EIS has been used in order to evaluate the thickness, the composition changes, formation of cracks, defects within oxide films and YSZ coatings during the oxidation process [18, 19]. In other words, when metallic samples with protective coatings are exposed to a non-aggressive electrolyte, the impedance response is unique essentially by the resistance and capacitance properties of the surface. Depending on the single or multilayer structure of the surface layer, the impedance spectra over a wide frequency range may exhibit two or more time constants [20]. The previous researches showed that the defects present inside the oxide or top coating contribute to electrolyte to penetrate into them. So, their electrical resistance will decrease. In the case of film breakthrough (caused by pitting) the electrolyte may reach to the substrate, and the overall electrical resistance across the film is remarkably decreased. A preliminary investigation showed that impedance of the oxide layer significantly decreases due to the presence of cracks inside the high-temperature oxide films [21].

The aim of this study is to use the EIS measurements for evaluating the characteristic of the oxide films formed on AZ91D magnesium alloy samples with an interlayer coating during different oxidation times. Oxidized samples for various times at 250 °C were exposed to an electrolyte and then EIS measurements were performed at open-circuit potential. Next, a physical model is proposed for the oxidized surface of the samples, and based on this model, an electrical equivalent circuit is fitted. Based on the data obtained from the model, the resistive and capacitive properties of the oxide films were evaluated. Meanwhile, their

variations with the oxidation times are related to the film growth and their defectiveness. Surface morphology and composition of the oxide films were examined using scanning electron microscopy (SEM) and X-ray diffraction (XRD), respectively.

2. Experimental method

2.1. Materials and solution

AZ91D magnesium alloy samples with dimensions of 12 mm × 12 mm× 2 mm were used as substrate in this study, and their composition is presented in Table 1. Before the coating process, the specimens were abraded progressively using emery papers of grade number 80 to 800. Subsequently, abraded specimens were degreased in acetone. Alkaline cleaning process was performed to remove any contamination. In the next step, plate-shaped aluminum powders (Hunan Hongyuan Co., China) with mean particle size of 5 µm, were used as an interlayer material. The aluminum powders (with concentration of 10 g/L) were dispersed in the ethanol solution under stirring. Then, a small quantity of $AlCl_3.6H_2O$ (0.6 mM) was added to the suspension in order to control the conductivity and enhance the dispersion of the suspension. Subsequently, the slurry was ultrasonically vibrated for 30 min to prepare a well-dispersed and stable suspension. The EPD process of the aluminum powders was conducted at an applied voltage of 30 V and deposition time of 3 min. An electrolytic cell with two electrodes was employed. The cathode was the magnesium alloy (substrate) and stainless steel 316L was used as the anode. The equivalent potential was produced by a set of two parallel-plane electrodes with 1 cm gap.

Finally, the 3YSZ powders (10 g/L) with mean particle size of 50 nm were dispersed in ethanol-acetyl acetone solution with 1:1 volume ratio and then were stirred. Also, I_2 (0.1 g/L) was added to the suspension as an additive to charge the particles in the suspension. The slurry was vibrated for 10 min using ultrasonic waves. Again, the magnesium alloy with the aluminum interlayer and the 316L stainless steel were selected as the cathode and anode in the EPD cell, respectively. The distance of the electrodes was fixed at 1 cm during the deposition. A voltage of 40 V was applied for the deposition of 3YSZ particles for 3 min. Then, the samples were heat-treated at 400±10 ºC in air for 60 min. The solutions were prepared using analytical grade chemicals (Merck Co.). Finally, the coated samples were oxidized in air at 250 °C for 1, 2, 3, 4, 5, 6, 7, 8, 9, and 10 h.

2.2. Electrochemical impedance spectroscopy (EIS)

To focus on the characteristics of the oxidized samples, a nonaggressive electrolyte, 0.1 M Na_2SO_4, was employed. A 3-electrode setup was used for the EIS tests at open circuit potential using a potentiostat/ galvanostat (EG & G, PARSTAT 2263) equipped with electrochemical impedance spectroscopy (EIS) module. In this setup, the oxidized samples were used as the working electrode. The auxiliary electrode and the reference electrode in the cell were 316L stainless steel and saturated calomel electrode (SCE), respectively. To perform these tests, a sinusoidal potential wave with 10 mV amplitude in the frequency range between 0.1 Hz to 100 kHz was applied to the samples. The samples were stabilized for 20 min in the solution prior to the EIS measurement. All experiments were performed at ambient temperature.

2.3. Characterization tests

The surface and cross-section of the samples were studied by scanning electron microscope (Tescan MIRA3 FEG-SEM, Czech Republic). In addition, the phase analysis of the samples was determined by X-ray diffraction (Equniox3000, France).

Table 1: Chemical composition of AZ91D used in this research.

Mg	Al	Zn	Mn	Cu	Ni	Fe
Bal.	8.3	0.35	0.12	0.03	0.002	0.005

3. Results and discussion

3.1. Impedance measurements

In impedance tests, electrodes with coatings were affected by a sinusoidal potential perturbation. Impedance diagrams can be extracted based on magnitude and phase shift of the current results. So, two types of impedance diagrams are used to interpret the received results of EIS analysis. In other words, the complex plane of impedance plot is called the Nyquist diagram. In the Nyquist diagram, the imaginary part of impedance is plotted against the real part. In this diagram, the real part of impedance is shown as Z' and the imaginary part is shown as Z'' and impedance is represented with the formula according to Eq. (1) [21]:

$$Z(\omega) = Z' + jZ'' \quad (1)$$

Furthermore, the impedance modulus versus frequency is defined by Bode plot and the phase part of impedance is demonstrated by phase part of Bode plot. The Bode plot at low frequencies is related to the polarization resistance, i.e. the resistance of oxide, or the resistance of coating. If a semicircle is characterized in Nyquist diagram, it could be attributed to impedance response of a simple resistor- capacitor (R-C). Moreover, the Nyquist plots are usually used to determine the important parameters of impedance results such as resistance and capacitance for an electrochemical system. In addition, if electrochemical system is complicated, it will be requisite to use an equivalent circuit model which can represent the microstructural characteristics of materials which are under study [7]. The typical Nyquist curves of the samples oxidized for different times are shown in Figure 1. In Nyquist plots, it can be recognized that in all cases, two semicircles can be determined in spectra. One at high frequencies (HF) and the other at medium frequencies (MF) which former could be attributed to YSZ coating and the latter could be related to the oxide film that has been formed during the oxidation process. Furthermore, a second curve or tail in Nyquist plots reveals an inductive behavior. The presence of inductive loop at low frequencies (LF) area of Nyquist curves can be attributed to the localized corrosion occurred around the AlMn phase in AZ91D alloy [1, 3, 22].

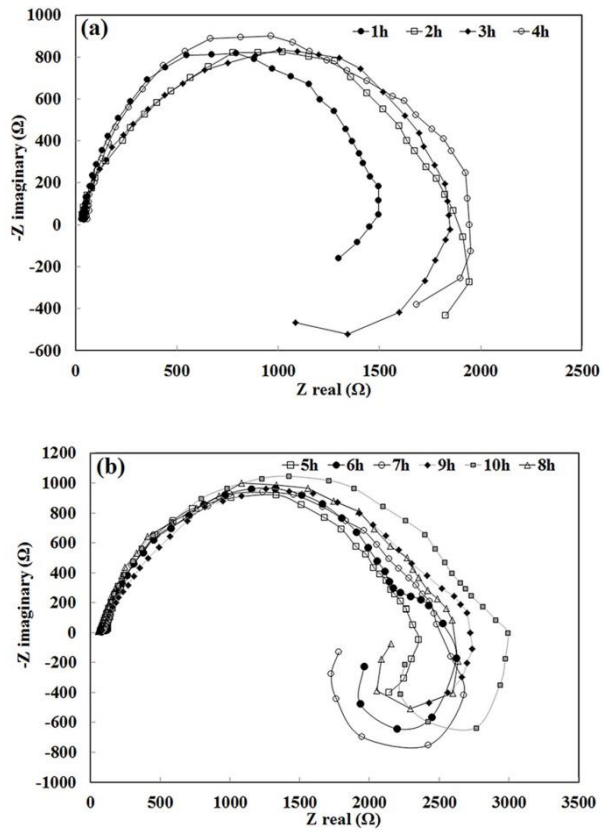

Figure 1: Typical Nyquist plots for the oxidized specimens exposed to 0.1M Na_2SO_4 solution. Oxidation temperature: 250 °C, (a) oxidized specimens for 1, 2, 3 and 4 h and (b) oxidized specimens for 5, 6, 7, 8, 9 and 10 h.

The Bode phase diagrams of the oxidized samples are shown in Figure 2. From this figure, it can be clearly seen that there are two time constants at high frequencies (HF) and medium frequencies (MF) regions which can be attributed to the presence of YSZ coating and oxide film, respectively. The positions of time constants at HF and MF in spectra are shown by arrows in Figure 2. Also, it can be confirmed that the time constant at MF could be superposition of both oxide film and electrode effect because it can be assumed that the oxide film is formed mainly from aluminum oxide. The electrical properties of this film are similar to those of magnesium oxides. So the time constant of aluminum oxide can overlap with the effect of electrode, magnesium oxide, or magnesium hydroxide response. In order to obtain the electrical properties of the oxide film, the spectra are usually fitted to an equivalent circuit which can correspond to an acceptable physical model of the system. The equivalent circuit can be selected to represent the electrical properties of the model with a high quality fitting. In addition, fitting of suitable equivalent circuit to measured spectra can be in high compliance [23]. Figure 3 depicts the physical model and corresponding equivalent circuit which have been used to interpret EIS spectra of oxidized samples. In this model, the both YSZ coating and oxide film which had been formed during oxidation process were considered as separate quasi-homogeneous phases and it is assumed that the films on oxidized samples have a sandwich-like structure [21].

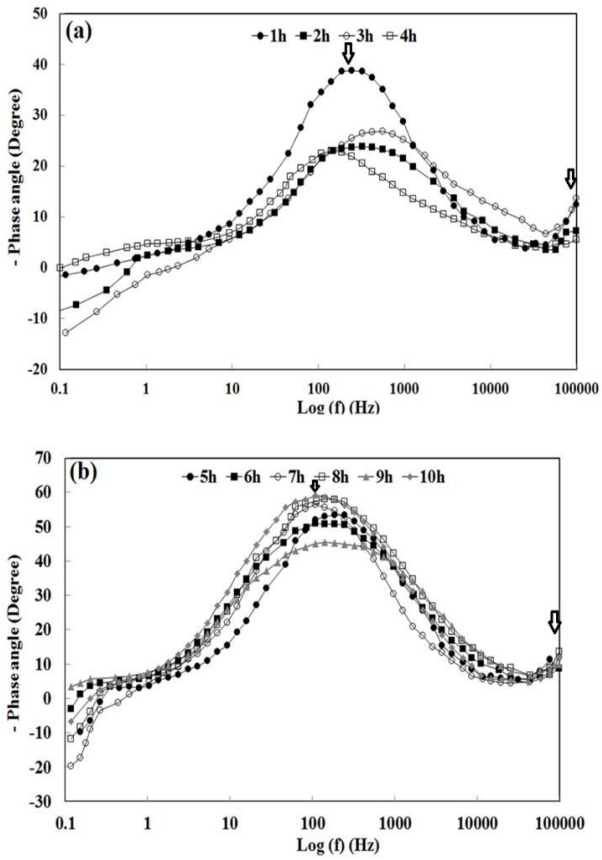

Figure 2: Phase angle as a function of frequency for the oxidized specimens exposed to 0.1M Na_2SO_4 solution. Oxidation temperature: 250 °C, (a) oxidized specimens for 1, 2, 3 and 4 h, and (b) oxidized specimens for 5, 6, 7, 8, 9 and 10 h.

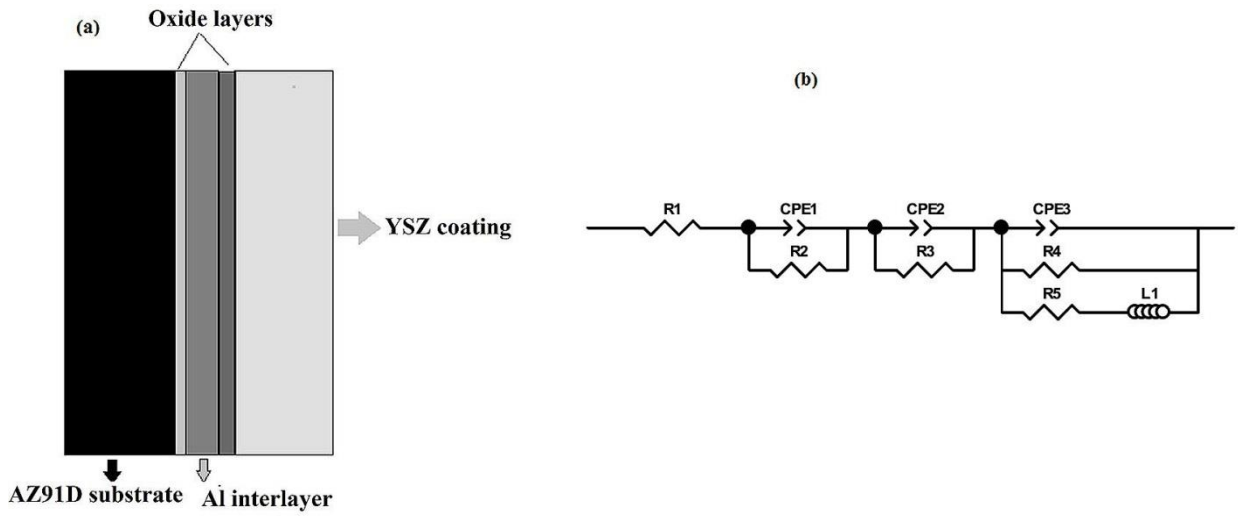

Figure 3: Schematic representation of the oxide models (a), the equivalent circuit for the interpretation of EIS spectra (b).

In Figure 3, R_1 is the electrolyte resistance, CPE_1 is the capacitance of the constant phase element (an indicator of the capacity of the coating), R_2 is the resistance of the coating, CPE_2 is also the capacitance of the constant phase element as an indicator of the capacity of the oxide film which has been formed during the oxidation process, and R_3 is the resistance of the oxide film. CPE_3 is the double layer constant phase element (an indicator of the double layer capacitance between the AZ91D alloy surface and the solution), R_4 is charge-transfer resistance of the corrosion reaction, L_1 is the inductance, and R_5 represents the inductance real resistance.

The equivalent circuit shown in Figure 3 was found to be mathematically satisfactory for the spectra fitting. According to Figure 4, there is a good compliance between the measured data and the fitted curves. Figure 4 displays the comparison between the measured data and fitted spectrum using the equivalent circuit which was shown in Figure 3. From Figure 4, it is clear that there is a good agreement.

In the equivalent circuit, CPE is the constant phase element which is more suitable to describe the behavior of a non-ideal capacitor where capacitance depends on frequency. For oxide film systems, the measured capacitive response is often not ideal and is not similar to a pure capacitor. This deviation is incorporated by utilizing a constant-phase element (CPE) instead of an ideal capacitance element. In general, the CPE could be corresponded to some types of heterogeneity of the surface or the surface film [24]. The impedance representation of CPE is given by Eq. (2):

$$Z_{CPE} = \frac{1}{[Y_0(j\omega)^n]} \quad (2)$$

In this equation, Z_{CPE} is the impedance of the constant phase element, in the ideal case, when the exponential factor n=1, the CPE acts like a capacitor with Y_0 equal to the capacitance C. ω stands for the frequency, n is the constant phase element exponent, and j is the imaginary unit. It should be mentioned that n varies between 0 and 1 [25].

On the other hand, the impedance parameters based on the suggested equivalent circuit were calculated using Zview software. By using the software's numerical methods, the fitted results are summarized in Table 2. In addition, the resistance (R_3) and capacitance of the oxide films (CPE_2 or Q_2) are represented in Figure 5 as a function of oxidation time. Clearly, it is seen from Figure 5 that the resistance of the oxide film is increased and capacitance is decreased with longer oxidation time. Also, the relationship between the resistance and capacitance with oxidation time is not absolutely linear. It can be due to the resistivity and dielectric constant changes with oxidation time.

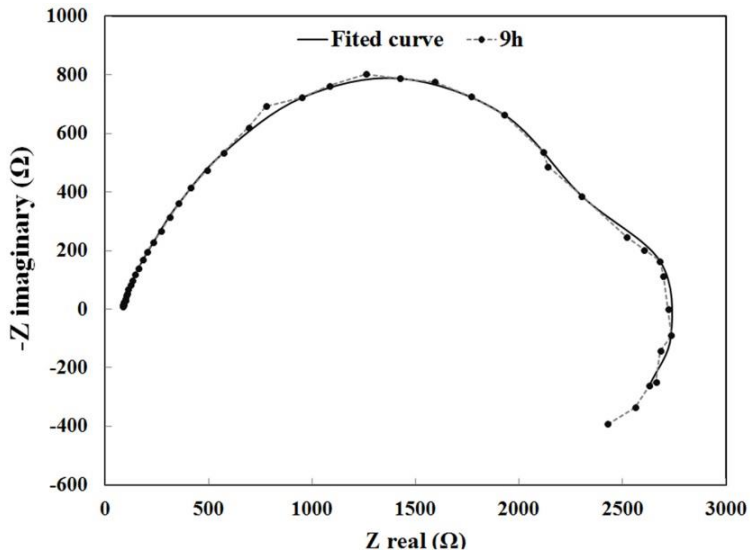

Figure 4: Comparison between the measured (dash line) and fitted spectra (solid line) for oxidized sample at 250 °C and time of 9 h.

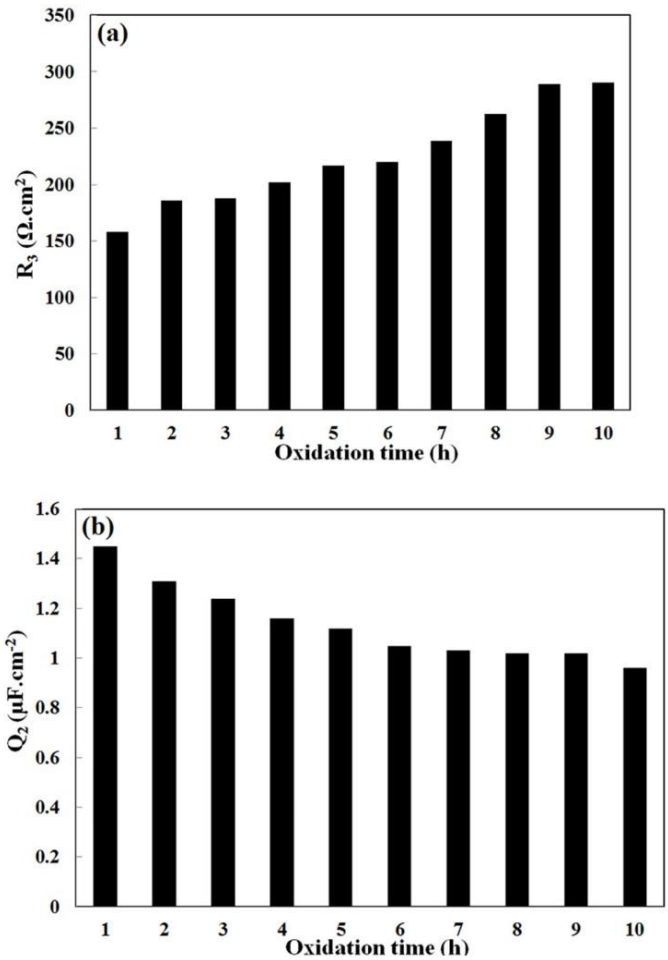

Figure 5: Resistance and capacitance of the oxide films based on the data of Table 2, (a) variation of oxide films resistance with oxidation time and (b) variation of capacitance of oxide films with oxidation time.

Table 2: Circuit element values calculated by fitting the model presented in Figure 3.

time (h)	R_1 ($\Omega.cm^2$)	CPE_1 ($\mu F.cm^{-2}$)	n_1	R_2 ($\Omega.cm^2$)	CPE_2 ($\mu F.cm^{-2}$)	n_2	R_3 ($\Omega.cm^2$)	CPE_3 ($\mu F.cm^{-2}$)	n_3	R_4 ($\Omega.cm^2$)	R_5 ($k\Omega.cm^2$)	L (kH/cm^2)
1	83.48	8.02	0.81	1384.37	1.45	0.91	158.11	2.05	0.71	120.0	0.32	2.45
2	86.83	7.21	0.92	1402.28	1.31	0.85	185.61	2.10	0.81	195.4	0.83	1.72
3	73.03	6.69	0.91	1447.52	1.24	0.75	187.77	3.38	0.80	136.7	0.64	1.54
4	74.14	5.67	0.79	1456.77	1.16	0.90	202.17	2.69	0.75	198.9	0.95	1.19
5	70.58	5.76	0.83	1549.36	1.12	0.90	216.86	3.45	0.70	174.8	0.43	1.26
6	79.81	5.15	0.76	1562.80	1.05	0.90	219.74	2.14	0.66	198.9	0.33	1.53
7	71.17	5.15	0.91	1500.97	1.03	0.90	239.04	1.42	0.65	152.9	0.72	1.06
8	70.91	5.21	0.91	1472.60	1.02	0.86	262.56	2.99	0.71	157.2	0.86	1.84
9	69.45	5.59	0.91	1465.25	1.02	0.91	288.86	3.56	0.69	100.2	0.14	1.21
10	70.32	5.38	0.90	1437.10	0.96	0.87	290.59	1.84	0.70	160.9	0.25	1.40

Also, it is expected that the greater oxide film resistance could be due to the thickening of the oxide film during the oxidation process. According to previous studies, the capacitance (C) and the resistance (R) of a homogenous oxide film can be calculated by Eq. (3) and (4) [21]:

$$C = \frac{\varepsilon\varepsilon_0 A}{d} \quad (3)$$

$$R = \frac{\rho d}{A} \quad (4)$$

where, A is the effective area, d is the thickness, ε_0 is the permittivity of vacuum, ε is the dielectric constant, and ρ is the resistivity of the oxide film. It is clear from these equations that with thickening of the oxide film, the resistance increases and the capacitance decreases. Also, during the oxidation process, the microstructure and composition of the oxide film can change and subsequently affects the dielectric constant. Figure 6 represents the resistance and capacitance of YSZ coating during the oxidation process, the resistance of YSZ coating increases till the oxidation time reaches to 6 h. With further increasing of the oxidation time, the resistance of YSZ coating decreases which can be due to the formation of defects such as pores, channels, or cracks inside YSZ coating. So, the defects prepare available ways for diffusion of oxygen to the substrate and then it increases the thickness of the oxide film during the oxidation process.

3.2. Microstructural analysis

The oxide layers that were formed on the AZ91D magnesium alloy with YSZ coating and aluminum interlayer at various oxidation times were characterized using a combination of two analytical techniques, i.e. SEM and XRD. By using these techniques, a complete picture of the structure of the oxidized samples was achieved. Figure 7 shows the SEM micrographs of the cross-sections of the as-received (not oxidized sample) and oxidized samples. It is seen that, there is no detectable oxide layer between the top coating (YSZ) and interlayer in as-received specimen; however, the XRD results which are presented in Figure 8 show the presence of Al_2O_3 and YSZ phases. It is assumed that the thickness of the oxide layer on as-received sample is low and it is not detectable by SEM technique. Also, a non-continuous oxide layer was formed on the surface of the sample oxidized for 3h. After oxidation for 6h, a continuous oxide layer was formed on the top coat/ interlayer interface. From Figure 8, it can be concluded that the oxide layer is mainly composed of Al_2O_3 phase and $MgAl_2O_4$ phases. Also, it is seen form Figure 5 and the results of XRD test that the thickness of the oxide layer was increased by increasing the oxidation time. It can be attributed to the increase of the pits, cracks, and holes density in YSZ coating.

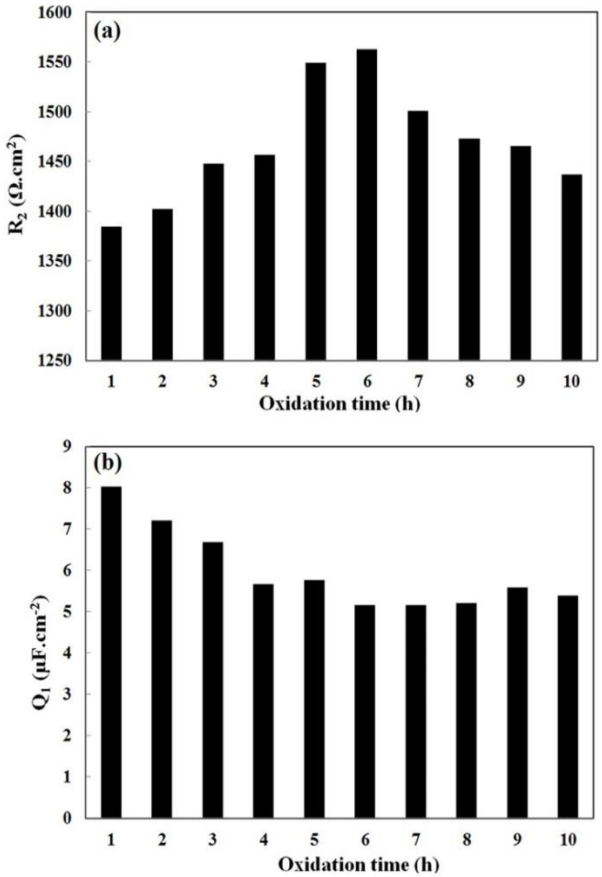

Figure 6: Resistance and capacitance of the YSZ coating based on data of Table 2, (a) variation of YSZ coating resistance with oxidation time and (b) variation of capacitance of YSZ coating with oxidation time.

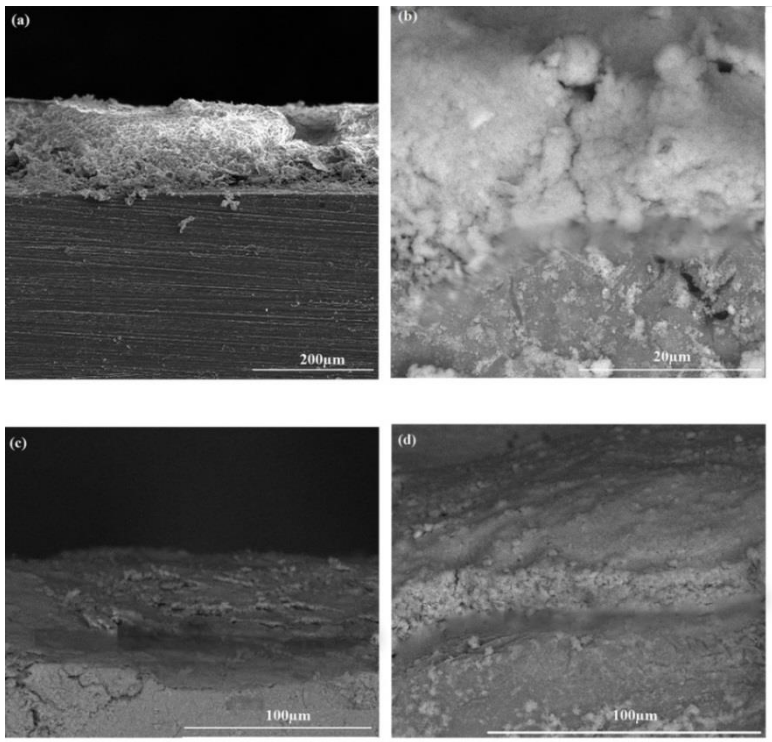

Figure 7: SEM micrographs of the cross-sections of (a) as-received, (b) oxidized samples for 3h, (c) 6h and (d) 9h at 250 °C.

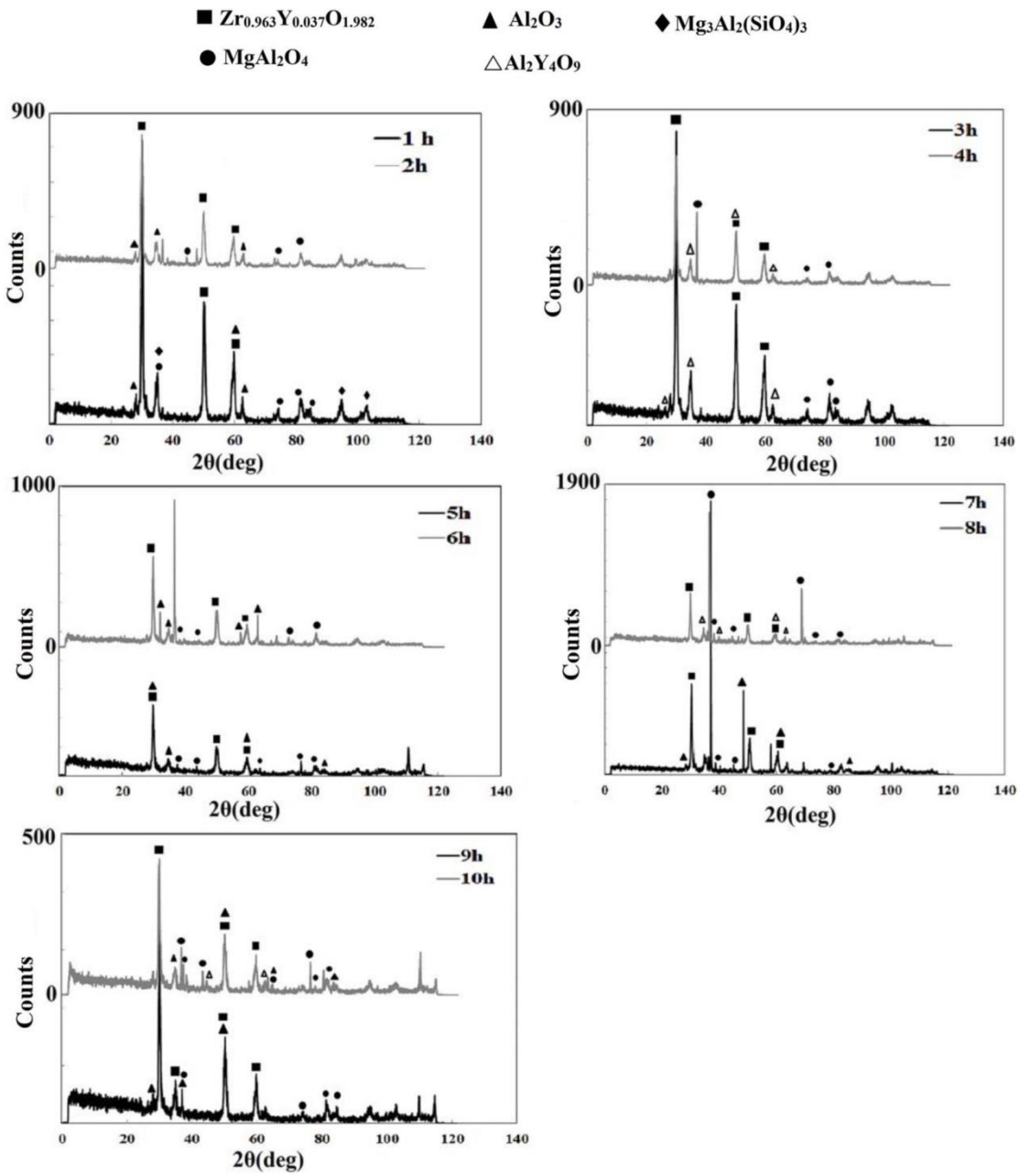

Figure 8: XRD pattern of oxidized specimens at 250 °C.

Figure 9 also depicts the surface morphologies of the oxidized samples. Figure 9 shows that the density of the cracks is increased in YSZ coating after 6h of oxidation process. The presence of cracks facilitates oxygen diffusion into interlayer and substrate and it increases the thickness of the oxide layer. Meanwhile, with increasing the oxidation time, the intensity of $MgAl_2O_4$ peaks also increases in XRD patterns that can be corresponded to an increase in phase volume.

The EIS results showed that the resistance of the oxide layer is increased with increasing the oxidation time, and SEM observations are in agreement with the EIS results. Furthermore, the EIS results showed that the capacitance of the oxide layer was almost constant. From the XRD results, it was certain that the phase composition of the oxide layer remained almost constant during the oxidation process.

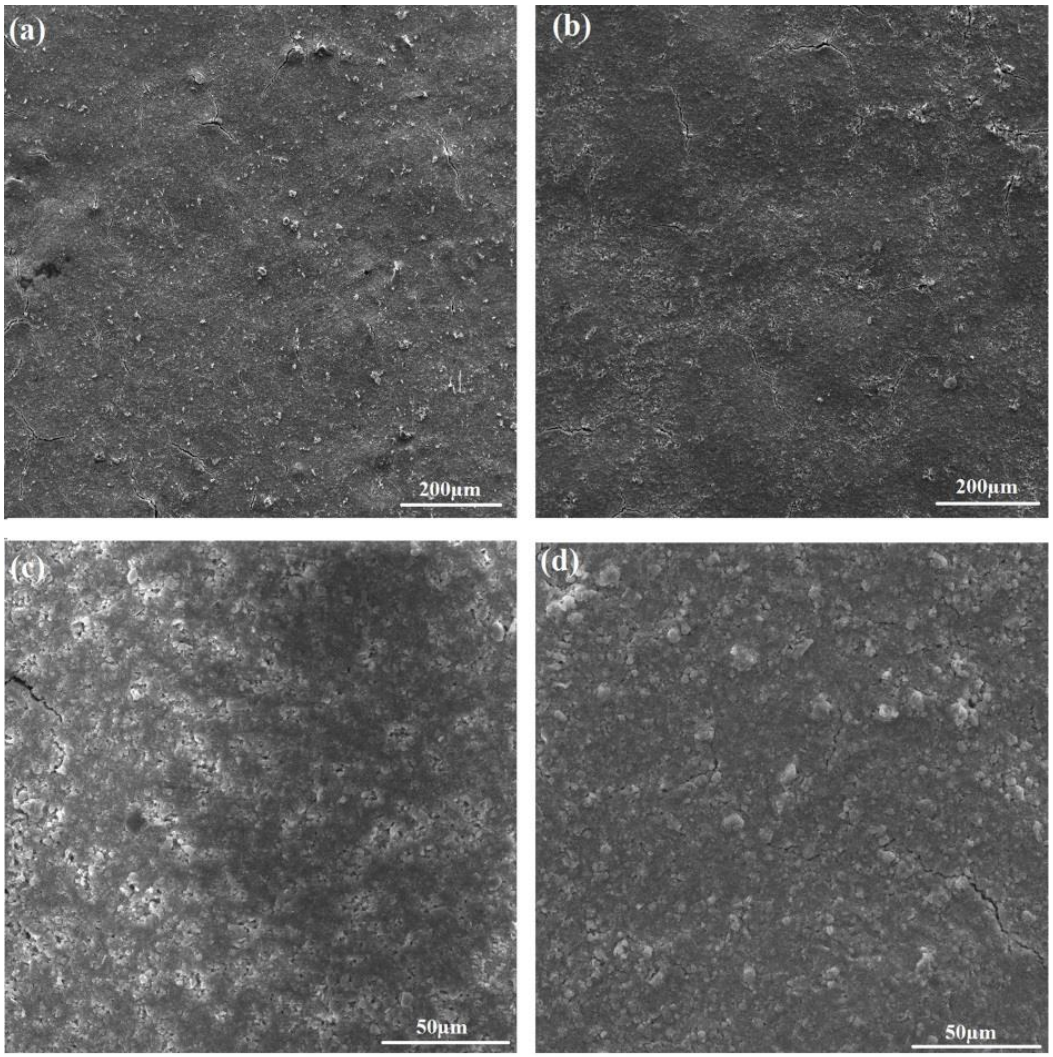

Figure 9: SEM micrograph of surface morphology of YSZ coatings after oxidation at 250 °C for (a) 2h, (b) 6h, (c) 8h and (d) 9h.

4. Conclusion

Oxidation of AZ91D magnesium alloy with YSZ coating and aluminum interlayer has been carried out in air at 250 °C. It was concluded that when the oxidation time is shorter than 6 h, a non-continuous oxide layer is formed between the top coating and interlayer. With further increasing of oxidation time, evaluation of SEM micrographs displayed that a continuous alumina scale was formed. In the impedance spectra, there are two time constants which correspond to the YSZ coating and the oxide layer. Impedance analyses demonstrate that the resistance of the oxide layer increases with oxidation time. This implies that the protective capability of the scale is enhanced with longer oxidation times. Also thickening of the oxide layer can be attributed to the increase of the density of cracks in YSZ coating because of increasing the oxidation time. In addition, the phase composition of the oxide layer remains almost constant during the oxidation process and it was mainly composed of $MgAl_2O_4$ and Aluminum oxide (Al_2O_3) phases.

Acknowledgments

The authors would gratefully like to thank Advanced Material Laboratory at the Central laboratory and Electrochemistry Laboratory at University of Tabriz who provided the valuable facilities for carrying out this research.

5. References

1. J. Chen, J. Wang, E. Han, J. Dong, W. Ke, Corrosion behavior of AZ91D magnesium alloy in sodium sulfate solution, *Mater Corrs*., 57 (2006), 789-793.
2. F. Czerwinski, The oxidation behaviour of an AZ91D magnesium alloy at high temperatures, *Acta Mater.*, 50 (2002), 2639-2654.
3. G. Baril, C. Blanc, N. Pébère, AC impedance spectroscopy in characterizing time-dependent corrosion of AZ91 and AM50 magnesium alloys characterization with respect to their microstructures, J *Electro Chem Soc.*, 148 (2001), B489-B496.
4. G.-L. Song, Corrosion of magnesium alloys, Woodhead Publishing Limited, *Philadelphia*, 2011, 3-57.
5. A. Pardo, M.C. Merino, A.E. Coy, R. Arrabal, F. Viejo, E. Matykina, Corrosion behaviour of magnesium/aluminium alloys in 3.5 wt.% NaCl, *Corros Sci*., 50 (2008), 823-834.
6. J. Gray, B. Luan, Protective coatings on magnesium and its alloys—a critical review, *J. Alloy Compad.*, 336 (2002), 88-113.
7. M.S. Ali, S. Song, P. Xiao, Evaluation of degradation of thermal barrier coatings using impedance spectroscopy, *J. Eur Ceram Soc*., 22 (2002), 101-107.
8. A. Shahriari, H. Aghajani, and M. Hosseini, Corrosion resistance enhancement of AZ91 magnesium alloy using Ni-P interlayer and electrophoretic deposited 3YSZ coating, *Prog. Color Colorants Coat*., 9 (2016), 151-162.
9. M.F. De Riccardis, Ceramic Coatings Obtained by Electrophoretic Deposition: Fundamentals, Models, Post-Deposition Processes and Applications, Intech Open Access Publisher, 2012, 43-68.
10. Z. Wang, P. Xiao, and J. Shemilt, Fabrication of composite coatings using a combination of electrochemical methods and reaction bonding process, *J. Eur Ceram Soc*., 20 (2000), 1469-1473.
11. J.A. Haynes, E. Douglas Rigney, K. Ferber, D. Porter, Oxidation and degradation of a plasma-sprayed thermal barrier coating system, *Surf. Coat. Technol.*, 86 (1996), 102-108.
12. J.M.West, Basic corrosion and oxidation, John Wiley & Sons, 1980, New york, 108-119.
13. L.L. Shreir, R. Jarman, G. Burstein, Metal/environment reactions: Corrosion, Butterworth Heinemann, London, 1994, 3-50.
14. P. Kofstad, High temperature corrosion, Elsevier Applied Science Publishers, London – New York, 1988, 5-38.
15. F. Mansfeld, Recording and analysis of AC impedance data for corrosion studies, *Corrosion*, 37 (1981), 301-307.
16. J. Macdonald, WB Johnson in: JR Macdonald (Ed.), Impedance Spectroscopy: Wiley, New York, 1987, 150-170.
17. N. Cogger, and N. Evans, An introduction to electrochemical impedance measurement technique report, no. 6. Solartron Instrument, 1999.
18. A.J. Bard, and L.R. Faulkner, Electrochemical methods: fundamentals and applications, Wiley, Chichester, 1980, 331-367.
19. X. Peng, D.R. Clarke, Piezospectroscopic analysis of interface debonding in thermal barrier coatings, *J. Am Ceram. Soc.*, 83 (2000), 1165-1170.
20. K. uttner, W. Lorenz, The role of surface inhomogenities in corrosion processes electrochemical impedance spectroscopy (EIS) on different aluminum oxide films, *Corros Sci.*, 29 (1989), 279-288.
21. J. Pan, C. Leygraf, R. F. A. Jargelius-Pettersson, J. Linden, Characterization of high-temperature oxide films on stainless steels by electrochemical-impedance spectroscopy, *Oxid Met*., 50 (1998), 431-455.
22. G. Baril, N. Pebere., The corrosion of pure magnesium in aerated and deaerated sodium sulphate solutions., *Corros Sci.*, 43 (2001), 471-484.
23. F. Mansfeld, Analysis and interpretation of EIS data for metals and alloys, Technical Report 26, Solartron - Schlumb erger, England, 1993.
24. S. Song, P. Xiao, An impedance spectroscopy study of high-temperature oxidation of thermal barrier coatings, *Mater. Sci. Eng: B.*, 97 (2003), 46-53.
25. JR. Macdonald, E. Barsoukov, Impedance spectroscopy: theory, experiment, and applications, Wiley & Sons, New Jersey , 2005, 87-90.

How to cite this article:
A. Shahriari, H. Aghajani, M. G. Hosseini,A Study of Oxidation Behavior of AZ91D Alloy with YSZ Coating Using EIS, Prog. Color Colorants Coat., 10 (2017), 1-12.

PROGRESS IN COLOR, COLORANTS AND COATINGS

available online @ www.pccc.icrc.ac.ir

Prog. Color Colorants Coat. 10 (2017), 67-72

Ministry of Science, Research and Technology
Institute for Color Science and Technology

مطالعه رفتار اکسایش آلیاژ AZ91D همراه با پوشش YSZ با استفاده از روش امپدانس الکتروشیمیایی

آیدا شهریاری[۱]، حسین آقاجانی[۲*]، میرقاسم حسینی[۳]

[۱] دانشجوی دکترا، دانشکده مهندسی مکانیک، دانشگاه تبریز، تبریز، ایران، صندوق پستی: ۱۶۴۷۱-۵۱۶۶۶.

[۲] دانشیار، دانشکده مهندسی مکانیک، دانشگاه تبریز، تبریز، ایران، صندوق پستی: ۱۶۴۷۱-۵۱۶۶۶.

[۳] استاد، دانشکده شیمی، دانشگاه تبریز، تبریز، ایران، صندوق پستی: ۱۶۴۷۱-۵۱۶۶۶.

چکیده

رفتار اکسایش آلیاژ منیزیمی AZ91D همراه با پوشش YSZ – آلومینیوم که در دمای ۲۵۰ درجه سانتی گراد در هوا اکسید شده بود، با استفاده از روش امپدانس الکتروشیمیایی (EIS)، میکروسکوپ الکترونی روبشی (SEM) و پراش اشعه ایکس (XRD) بررسی شد. اکسایش در زمان‌های ۱ تا ۱۰ ساعت انجام شد. از سل سه الکترودی به منظور آزمون EIS بر روی نمونه‌های اکسید شده در محلول غیر خورنده ۰/۱ مولار Na_2SO_4 استفاده شد. داده‌های امپدانسی حاصل با استفاده از یک مدل دولایه تفسیر شدند و تغییرات مقاومت و ظرفیت خازنی به تغییرات در ضخامت و عیوب در پوشش زیرکونیایی و فیلم اکسیدی تشکیل شده در طی اکسایش نسبت داده شد. نتایج نشان داد که بعد از ۶ ساعت از اکسایش، عیوب در داخل پوشش زیرکونیایی ایجاد می‌شود که این عیوب به عنوان راهی برای افزایش دریافت اکسیژن و در نهایت افزایش ضخامت فیلم اکسیدی شکل گرفته کمک می‌کنند. همچنین، نتایج XRD نشان داد که ترکیب اصلی فیلم اکسید از Al_2O_3 و $MgAl_2O_4$ تشکیل شده است. فیلم اکسیدی در طی زمان اکسایش محافظ باقی می‌ماند. به علاوه، مدل الکتروشیمیایی پیشنهاد شده با مشاهدات میکروسکوپ الکترونی در توافق است.

اطلاعات مقاله

تاریخچه مقاله:

تاریخ دریافت: ۱۲ شهریور ۱۳۹۵

تاریخ دریافت آخرین اصلاحات: ۹ آبان ۱۳۹۵

تاریخ پذیرش: ۲۳ آبان ۱۳۹۵

تاریخ در دسترس به صورت الکترونیکی از: ۳۰ آذر ۱۳۹۵

واژه‌های کلیدی:

امپدانس الکتروشیمیایی

فیلم اکسیدی

AZ91

YSZ

*Corresponding author: h_aghajani@tabrizu.ac.ir